Double electron–electron resonance with multiple non-selective chirp refocusing

Originally published in:
Physical Chemistry Chemical Physics 19(2), https://doi.org/10.1039/c6cp07262c

Funding acknowledgement:
157034 - Nanometer-range distance constraints for biomolecular complexes - Measurement, uncertainty estimates, and use in modeling (SNF)

Double electron-electron resonance with multiple non-selective chirp refocusing†

Andrin Doll,*‡ and Gunnar Jeschke

Received Xth XXXXXXXXXX 20XX, Accepted Xth XXXXXXXXX 20XX
First published on the web Xth XXXXXXXXXX 200X
DOI: 10.1039/b000000x

A new approach to double electron-electron resonance (DEER) for distance determination involving nitroxide spin labels at dilute concentrations is presented. In general, DEER pulse sequences rely on double resonance between pump and observer spins excited by selective pulses at two distinct microwave frequencies. In the new approach abbreviated as nDEER, non-selective chirp pulses that refocus all relevant spin pairs are combined with DEER. This non-selective refocusing results in suppression of unmodulated contributions, such as the constant contribution as well as the background curvature due to inter-molecular spin partners in ordinary DEER data. Due to this dipolar attenuation effect, primary nDEER data are closer to the dipolar modulation of primary interest than ordinary DEER data. Restrictions of nDEER are that secondary information related to these unmodulated contributions becomes difficult to retrieve. Accordingly, incomplete deconvolution of the inter-molecular background prevents the application of nDEER to rigid spin pairs at high concentrations. A key advantage of nDEER is the high fidelity of the chirp refocusing pulses, which is important for nDEER schemes that incorporate dynamical decoupling to access longer distances. In this context, nDEER with Carr-Purcell (CP) pulse trains having $N = 2$ and $N = 4$ refocusing pulses are demonstrated. These CP nDEER sequences require a total of $N + 2$ pulses, which is less than the $2N + 1$ pulses required for CP DEER schemes. The pump pulse position is incremented throughout the refocusing pulses, which restricts the minimum time increment to 96 ns on our spectrometer and therefore complicates application to distances below 3 nm. At Q-band frequencies, unwanted modulations related to pulse imperfections contribute only 3.5% relative to the principal nDEER modulation. Accordingly, there is no need for dedicated data reconstruction methods as in CP DEER methods.

1 Introduction

Electron paramagnetic resonance (EPR) techniques based on pulsed microwave excitation allow for spectroscopic separation of the dipolar interaction between electron spins. This capability has become a reliable tool for determining spatial spin conformations in the lower nanometer range. In particular, structural information can be obtained from biomacromolecules containing native paramagnetic co-factors or spin tags introduced by site-directed mutagenesis[1–4]. The most common approach employs diamagnetic molecules labeled with a pair of nitroxide spin labels. For such samples, inter-spin distances ranging from 2 nm to 8 nm can be probed using established techniques[5].

A wide-spread pulse sequence for time-variable evolution under the dipolar interaction is the four-pulse double electron-electron resonance (DEER) sequence[6]. This sequence is based on the principle of double-resonance[7], where pulses at two distinct frequencies are applied to observe and pump the spins. The spin dynamics of this experiment are controlled by pulses which can excite each of two coupled spin partners individually. Accordingly, DEER is based on selective pulses[8]. There are also other pulse sequences where the spin dynamics are due to non-selective pulses that excite both coupled spins simultaneously[9]. Contemporary examples include the six-pulse double-quantum coherence (DQC) experiment[10] and the four-pulse single-frequency technique for refocusing dipolar couplings (SIFTER)[11]. A challenge in these experiments is that non-selective pulses should excite the entire EPR spectrum for best data quality, which is barely possible for nitroxides using monochromatic pulses that excite at most a bandwidth of 100 MHz[4,12].

Within the last decade, fast arbitrary waveform generators (AWG) made pulse shaping at microwave frequencies possible[13–15]. For pulsed EPR, this led to enhanced excitation bandwidth by means of either optimal-control pulses[16] or frequency-swept (chirp) pulses[17,18]. The majority of such experiments to date were performed using frequency-swept

† Electronic Supplementary Information (ESI) available: Pictorial representations of evolution pathways, rationale for non-selective refocusing, general modulation formula, dipolar attenuation within the inter-molecular background, quantification of pulse skipping artifacts, spurious dipolar evolution pathways, quantification of spurious dipolar modulation, echo decays for nDEER and DEER. See DOI: 10.1039/b000000x/

Laboratory of Physical Chemistry, ETH Zurich, Vladimir-Prelog-Weg 2, 8093 Zurich, Switzerland. E-mail: andrin.doll@alumni.ethz.ch
‡ Present address: Service de physique de l'état condensé, CEA Saclay, 91191 Gif-sur-Yvette, France.

pulses, which previously found a number of application in nuclear magnetic resonance experiments[19]. In general, the performance of frequency-swept pulses can be characterized by means of their (minimum) adiabaticity factor Q_{crit}[20]. Within Landau-Zener-Stückelberg-Majorana (LZSM) theory[21,22], an equivalent pulse flip angle β_{LZSM} due to the passage through the resonance condition can be computed from Q_{crit}, which serves as an estimate for the experimental flip angle[23].

With respect to distance determination, the substitution of monochromatic pulses by broadband frequency-swept pulses brought several improvements. First, chirp pump pulses in DEER and related experiments revealed enhanced dipolar modulation depths when pumping spins with a broad spectral distribution, such as transition metal or lanthanide ions[17,18,24–26]. Second, the broader excitation bandwidth of the pulses considerably improved data quality of SIFTER experiments using nitroxides[27] and has put two-dimensional extensions thereof within reach[28]. Third, shaped pump pulses turned out to be favorable for DEER sequences with multiple pump pulses that incorporate dynamical decoupling[29,30]. These sequences aim for a longer phase memory time to access longer inter-spin distances by employing a Carr-Purcell (CP) train of N refocusing pulses[29]. In particular, the CP train refocuses temporal fluctuations of the hyperfine fields of surrounding nuclei having fluctuation time scales on the order of the pulse spacing[31,32]. However, these pulse sequences require N pump pulses which should ideally flip the pumped spins N times with probability close to 100%. The pump pulses thus require a highly frequency-selective excitation profile, especially for $N > 2$. To date, the largest N of three has been achieved by the seven-pulse DEER sequence using three frequency-selective pump pulses with hyperbolic-secant modulation functions[30]. In all CP DEER results presented so far, non-ideal performance of the pump pulses introduced artifacts with amplitudes beyond the noise level[18,29,30,33], so that dedicated post-processing[30] or additional experiments[29] are required.

In this work, we aim for a new pulse sequence that shows better scaling towards dynamical decoupling than the previous approaches. This new sequence is based on both non-selective and selective pulses. In this way, the sequence still employs double resonance between pumped and observed spins as defined by selective pulses at two frequencies. However, all refocusing pulses are non-selective and invert both the pumped and the observed spins. In particular, the refocusing pulses in DEER sequences are substituted by chirp pulses having a bandwidth that covers both the observed and the pumped spins. The pump pulse as well as the first observer $\pi/2$ remain monochromatic pulses. We refer to the resulting pulse sequences as non-selective DEER, which is abbreviated by nDEER.

Experimentally, nDEER sequences were tested with a rigid nitroxide ruler using a high-power AWG spectrometer at Q-band frequencies around 34 GHz, as described in Section 2. The differences between ordinary four-pulse DEER and the corresponding nDEER sequence with two chirp refocusing pulses are analyzed in Section 3. In this context, we will refer to four-pulse DEER as DEER4, whereas the nDEER equivalent will be referred to as nDEER4. In Section 3.1, we constitute four apparent differences between primary data of DEER4 and nDEER4. The theoretical analysis that follows in Section 3.2 explains these four experimental observations and additional aspects specific to nDEER.

The extension of nDEER to dynamical decoupling is presented in Section 4, where sequences with up to $N = 4$ non-selective refocusing pulses will be demonstrated experimentally. For these sequences, we will use the nomenclature CP2-nDEER and CP4-nDEER to refer to nDEER with $N = 2$ and $N = 4$ refocusing pulses, respectively.

2 Materials and Methods

2.1 Sample preparation

A nitroxide-ruler holding two nitroxide spin labels at a distance of about 4.0 nm was used. The synthesis and EPR characterization of this ruler are detailed elsewhere[34,35]. The chemical structure of the ruler is shown below in Fig. 1. For all EPR experiments, the compound has been dissolved to a concentration of 50 μM in a deuterated ortho-terphenyl matrix, which provided extended phase memory times around 21 μs at the measurement temperature of 50 K. Prior to glass formation by shock-freezing in liquid nitrogen, the sample tube was heated beyond the melting point of ortho-terphenyl around 60° C.

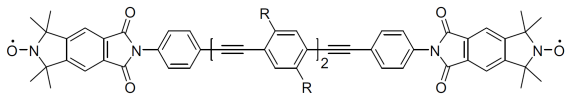

Fig. 1 Structure of the nitroxide-ruler used in this study[34,35].

2.2 Experimental

All Q-band experiments have been performed on a home-built high-power ultra-wideband X/Q-band AWG spectrometer[28,36]. This spectrometer features versatile pulse sequence programming and synthesis by a 8 GSa/s AWG as well as acquisition of averaged echo transients with a short data transfer time on the order of 1 ms. A home-built loop-gap resonator having a loaded quality factor around 120 and accepting 1.6 mm outer-diameter sample tubes was used. The measurement temperature was 50 K and the repetition time was 4 ms. The

static field was set to 1.243 T, unless the experiment required a swept field. Under these conditions, the nominal pulse power of 200 W delivered by the power amplifier provided peak field strengths ν_1 up to 110 MHz for spin excitation.

Monochromatic pulses for selective excitation or refocusing had durations of 12 ns and the frequency separation between pump and observer was 100 MHz (see also Fig. 2b). The non-selective chirp refocusing pulses for nDEER swept their frequency over a range of $\Delta f = 330$ MHz and compensated for the experimental resonator profile $\nu_1(f)$ by adaptation of the frequency modulation function[17]. These pulses had durations of 64 ns and the leading and trailing flanks were apodized sinusoidally during $t_{\mathrm{rise}} = 10$ ns[37]. With these parameters, a critical adiabaticity $Q_{\mathrm{crit}} = 8.0$ was achieved. For a two level system, this corresponds to an adiabatic pulse with a nominal flip angle $\beta_{\mathrm{LZSM}} = 179.79°$[23].

The sequence timings used for DEER and nDEER experiments using the selective and non-selective pulses described above are illustrated graphically aside the experimental results. The values for the timings are found in the corresponding figure captions. These sequences have in common that the dipolar evolution time t was incremented in steps of $\Delta t = 96$ ns. With a net evolution window on the order of 22 μs, as used predominantly within this study, the dipolar modulation was therefore sampled by at least 230 data points. Moreover, the raster was set such that more than three of these data points sampled the dipolar evolution for negative t for dead time free acquisition. For nDEER, the time raster of the pump pulse was chosen such that there was always a time gap of at least t_{gap} = 10 ns between the pump pulse and any of the non-selective refocusing pulses. To fulfill this criterion for all refocusing pulses, the delay between subsequent refocusing pulses was set to a multiple of $2\Delta t$.

Unless explicitly indicated otherwise, the high-power amplifier has been left in its active state during application of the pulses, i.e. from the first until the last pulse. For pulse sequences with total duration beyond 54 μs, echoes vanished abruptly due to a gating limitation of our high-power amplifier. In principle, it is possible to circumvent such limitations by gating each pulse individually. However, we would expect complications of such an approach with respect to the CP nDEER sequences that are presented in Section 4, where pulse skipping would merge the gates into one single gate. On our spectrometer, this instrumental limitation currently restricts the maximum time window that can be recorded by CP2-nDEER and CP4-nDEER to 36 μs and 31 μs, respectively. See also Section 5 of the ESI† for a potential workaround.

Phase cycling was used to reject unwanted coherence transfer pathways. For the non-selective CP refocusing pulse trains, we made use of two-step and four-step cycles to select coherence order changes of 2, namely o2.2 = [+(+x) +(-x)] and o2.4 = [+(+x) -(+y) +(-x) -(-y)]. Here and in the following, oc.n denotes a phase cycle that selects order c and has n steps. We applied the o2.2 cycle to the first refocusing pulse in the case of two refocusing pulses[5]. In the case of four refocusing pulses, the o2.2 cycle was applied to the third pulse and the o2.4 cycle to the preceding two pulses[5]. In every DEER and nDEER experiment, we additionally cycled the first pulse by an o1.2 = [+(+x) -(-x)] cycle. Moreover, since the coherent pump pulse on our spectrometer causes additional echoes[33], the pump pulse was cycled by the four-step cycle o0.4 = [+(+x) +(+y) +(-x) +(-y)].

Overall, an ordinary four-pulse DEER experiment thus had an eight-step cycle. For nDEER with four refocusing pulses, 256 phase cycling steps resulted. To compare the various experiments at an identical number of sequence repetitions, the shots per data point have been adapted. Accordingly, DEER was acquired with 128 shots per point, while nDEER with four refocusing pulses was acquired with 4 shots per point. The number of total sequence repetitions, i.e. the number of sequence averages, is indicated in the figure captions, where experimental data are presented. With our typical parameters, acquisition of one single average took on the order of 15 minutes.

Notice that while an experiment was running, there were no delays due to data transfer, since averaged echo transients were transferred to the host computer within the sequence repetition time of 4 ms, even if only 4 shots per point were used. Our spectrometer can therefore acquire echo transients of nitroxides without noticeable interrupts, which is a feature that is missing on other pulsed EPR spectrometers available in our lab.

However, the increased number of phase cycles expressed itself during sequence compilation. In particular, a typical nDEER pulse sequence with four refocusing pulses needed to be performed as two experiments with 128 phase cycling steps each. Each of these sub-blocks required 354 MSa of digital data to be synthesized by the AWG, which corresponded to 17% of the available digital data memory on our AWG. Moreover, the 354 MSa of digital data was segmented in $2^{18.82}$ individual blocks, where the maximum number of such individual blocks on our AWG was 2^{19}. The preparation of such a pulse sequence required 76 s, where most of the time was spent on the host computer to calculate the digital waveforms that define the entire pulse sequence. For DEER4, the preparation time of the entire experiment was only 9 s, since the smaller number of phase cycles and pulses required less digital waveforms to be computed.

3 Dipolar modulation with non-selective refocusing

3.1 Experimental results

In order to analyze the spin dynamics under non-selective refocusing, ordinary four-pulse DEER experiments (DEER4) are compared to four-pulse DEER with non-selective refocusing (nDEER4). The pulse sequence used for this purpose is illustrated in Fig. 2a. The upper part of the illustration depicts the timing of the four pulses. In the lower part, the pulses used in DEER4 and nDEER4 are differentiated by their color coding. In particular, the refocusing pulses ② and ④ are different in DEER4 and in nDEER4, whereas the pulses ① and ③ as well as the pulse timing are identical.

The experimentally obtained excitation profiles of the pulses used in DEER4 and nDEER4 are illustrated in the upper part of Fig. 2b, where the color coding from panel a is used. The monochromatic pulses were centered with respect to the pump and observer frequencies at 34.8 GHz and 34.9 GHz, respectively. In analogy to our previous work at X band[36], the peak inversion efficiency related to frequency-swept pulses was larger than the peak inversion efficiency related to monochromatic pulses. Nevertheless, the experimental inversion efficiency of the chirp refocusing pulse was below the theoretical expectation for a two-level system. In particular, one would expect an inversion efficiency of 99.9997% for the critical adiabaticity $Q_{\mathrm{crit}} = 8$ achieved by the Q-band pulse[23]. Experimentally, however, the inversion efficiency ranges from 96% to 98%. For nitroxides at X-band frequencies, larger experimental inversion efficiencies virtually reaching 100% have been observed (see Fig. 1 in ref.[36]).

The lower part of Fig. 2b shows the positioning of all pulse excitation profiles with respect to the nitroxide spectrum (black) and with respect to the resonator profile (gray). The black asterisk marks a spectral impurity due to E' centers in the clear fused quartz sample tube.

For both DEER4 and nDEER4, the timing t of the pump pulse can be set such that evolution under the dipolar coupling is refocused. For DEER4, this corresponds to $t = 0$ and the real component of the FT of the spin echo obtained at $t = 0$ is shown in orange in Fig. 2c. The frequency offset along the abscissa is here the frequency difference with respect to the observation frequency. The spectral impurity is also seen in this FT spectrum and is again indicated by an asterisk. For nDEER4, the dipolar evolution is refocused for $t = \tau_2 - \tau_1$ (see below) and the FT of the spin echo in this case is illustrated by the solid blue curve in panel c. The dashed blue curve is the FT echo spectrum acquired in absence of the pump pulse ③.

To exclude the spectral impurity in DEER results, the spin echoes were evaluated by integration of the FT spectrum over a range from 0 MHz to 75 MHz frequency offset (see the hor-

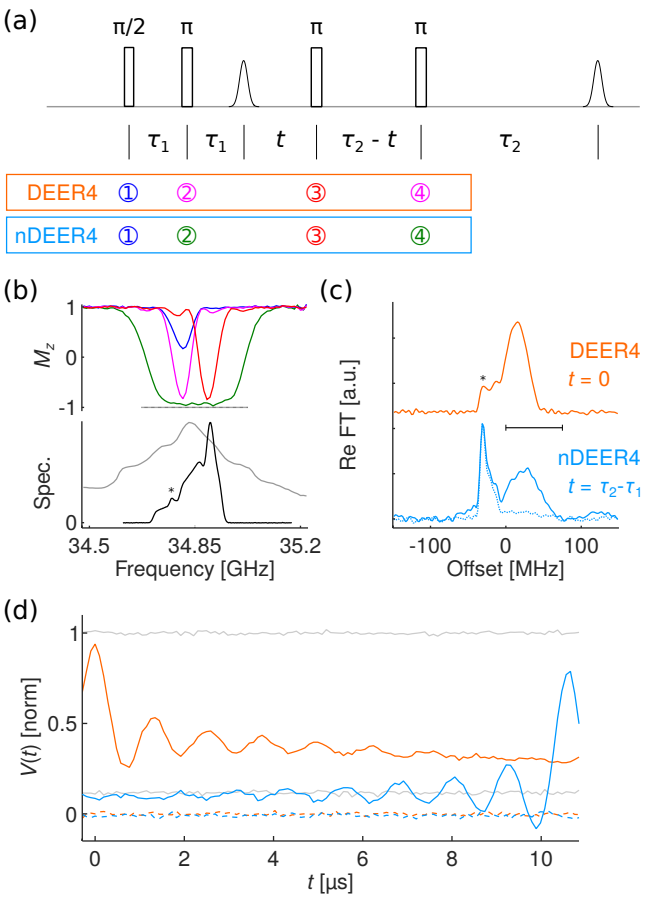

Fig. 2 The four-pulse DEER sequence with selective (DEER4) and non-selective (nDEER4) refocusing. **(a)** Pulse sequence timing, where $\tau_1 = 400$ ns and $\tau_2 = 11$ μs was used. The Gaussian profiles indicate the primary and the refocused primary echo. The pulses have their flip angles indicated above. The pulse labels ① - ④ as used for DEER4 and nDEER4 are color-coded at the bottom. **(b, top)** Experimental pulse profiles, using the color coding of panel a. **(b, bottom)** Field-swept spectrum cast in frequency scale (black) and experimental resonator profile $\nu_1(f)$ (gray). The asterisk denotes a spectral impurity originating from E' centers in the sample tube. **(c)** Real component of the FT of the DEER4 (orange) and nDEER4 (blue) refocused primary echo. The solid curves were recorded at $t = 0$ and $t = \tau_2 - \tau_1$, respectively. The abscissa denotes the offset with respect to the observation frequency. The dashed blue curve is the nDEER4 echo without the pump pulse ③. The black horizontal ruler denotes the 75 MHz frequency integration range used to determine echo amplitudes $V(t)$. The asterisk denotes the position of the spectral impurity. **(d)** Real (solid) and imaginary (dashed) components of DEER4 and nDEER4 signal, with color coding as in panel c. The two horizontal gray curves correspond to DEER4 (upper curve) and nDEER4 (lower curve) recorded without the pump pulse ③. All data recorded within 15 min each (one sequence average) and normalized to DEER4 without pump.

izontal ruler). Up to differences in the spectral amplitudes between the DEER4 and nDEER4 echo FT, the nDEER4 echo signal had a larger bandwidth as compared to the DEER4 echo, which is explained by the increased inversion bandwidth of the refocusing pulses (see panel b). Moreover, the maximum of the FT of the nitroxide echo is not centered at zero frequency offset with respect to the observation frequency, both for DEER4 and nDEER4. This is due to the nitroxide lineshape and due to the frequency-dependent coupling by the resonator.

Fig. 2d shows real (solid) and imaginary (dashed) components of the DEER4 (orange) and the nDEER4 (blue) signal. Both curves were obtained by integration of the FT echo spectra as detailed in panel c. In addition to the principal DEER4 and nDEER4 signals, two curves are shown in gray. The upper curve corresponds to DEER4 without the pump pulse ③ and serves as normalization for all data shown in this plot. The lower curve is the echo amplitude of nDEER4 in absence of the pump pulse ③.

Based on these experimental results, we make the following observations:

I. The dipolar evolution in DEER4 and nDEER4 is refocused at different times t. With the four-pulse DEER sequence timing in particular, the nDEER4 signal refocuses (almost) at the end of the DEER4 trace, and vice versa.

II. The pump pulse in DEER4 results in a reduction of the echo amplitude due to dipolar modulation and off-resonance effects, as is seen when comparing the signals with and without the pump pulse ③. In nDEER4, this situation appears reverse. In particular, the pump pulse results in a larger echo.

III. Even though the same pump pulse has been used for both DEER4 and nDEER4, the apparent modulation depth of nDEER4 is larger than for DEER4. However, the echo amplitude for nDEER4 is smaller than for DEER4.

IV. The nDEER4 signal has a less pronounced background decay as compared to the DEER4 signal. While the DEER4 background decay can be readily identified in the plot, the decay contribution in nDEER4 is difficult to identify, even when comparing between the modulated signal and the unmodulated signal in absence of the pump pulse ③.

3.2 Theoretical considerations

In order to explain the experimental observations above, the dipolar modulation in DEER4 and nDEER4 is analyzed theoretically. As will become clear further below, observations *I* - *III* can be understood by considering a pair of coupled spins (Section 3.2.1). To explain observation *IV*, effects related to multiple spin partners need to be taken into account (Section 3.2.2). The analysis of the dipolar modulation is based on mathematical expressions verified by product operator formalism[38]. To complement the mathematical description, pictorial phase evolution diagrams[39] are presented in Section 1 of the ESI†.

The consequences of using frequency-swept refocusing pulses are analyzed in Section 3.2.3 and in Section 2 of the ESI†.

3.2.1 Modulation formula for two spins. For two coupled spin partners, we consider the (weak coupling) Hamiltonian

$$\hat{\mathscr{H}}_0 = \Omega_1 \hat{S}_{1,z} + \Omega_2 \hat{S}_{2,z} + \omega_{12} \hat{S}_{1,z} \hat{S}_{2,z} \tag{1}$$

where Ω_1 and Ω_2 are the resonance offsets of the observed and the pumped spin, respectively, with respect to a rotating frame. The angular frequency ω_{12} is the dipole-dipole coupling between the two electron spins. In the following analysis, we consider all pulses to be either perfectly selective with respect to the observed spin S_1 and the pumped spin S_2, or perfectly non-selective. Moreover, we neglect any effects related to the frequency sweep of the non-selective pulses. These effects are considered later in Section 3.2.3. In this case, the dipolar modulation formulas of the DEER4 and nDEER4 echoes, at the time instant where the resonance offsets refocus, are

$$V_{\mathrm{DEER4}}(t)|_{\mathrm{main}} = \cos(\omega_{12} \cdot t) \tag{2}$$

$$V_{\mathrm{nDEER4}}(t)|_{\mathrm{main}} = \cos(\omega_{12} \cdot (t - \tau_2 + \tau_1)) \tag{3}$$

The dipolar modulation has therefore its zero point at $t = 0$ for DEER4 and at $t = \tau_2 - \tau_1$ for nDEER4, which explains the different refocusing times observed experimentally (observation *I*). In fact, the nDEER4 evolution pathway that refocuses towards the end of the DEER4 signal at $t = \tau_2 - \tau_1$ is a residual artifact in experimental data due to pulse imperfections and spectral overlap[40] (see *"inversion pattern 8"* in Table 1 of ref.[40]). Moreover, the '2+1' experiment is a *mixed* case, since dipolar evolution pathways with selective refocusing as well as with non-selective refocusing contribute significantly to the '2+1' signal[41].

For observation *II*, namely the different DEER4 and nDEER4 echo intensities in absence of the pump pulse, we consider the dipolar evolution if the coupled spin is not inverted. In this case, we find

$$V_{\mathrm{DEER4}}(t)|_{\mathrm{no\ pump}} = 1 \tag{4}$$

$$V_{\mathrm{nDEER4}}(t)|_{\mathrm{no\ pump}} = \cos(\omega_{12} \cdot \tau_{\mathrm{sum}}) \tag{5}$$

where $\tau_{\mathrm{sum}} = \tau_1 + \tau_2$. Both signals are unmodulated, since they do not show any dependence on t. Nevertheless, nDEER4 causes dipolar evolution throughout the entire time window in absence of the pump pulse. This is due the inability to refocus the dipolar evolution with non-selective refocusing pulses[8]. Essentially, the dipolar evolution in nDEER4 is refocused by

the pump pulse. In DEER4, the role of the pump pulse is exactly opposite, since the pump pulse introduces time-variable defocusing of the dipolar evolution (whereas the selective refocusing pulses refocus the dipolar evolution).

In order to relate Eq. (5) to observation *II*, ensemble averaging over a distribution of dipolar frequencies ω_{12} needs to be taken into consideration. For the case that the time window τ_{sum} is larger than the involved inverse frequencies $2\pi/\omega_{12}$, the signal in absence of the pump pulse is indeed attenuated significantly as compared to the signal in presence of the pump pulse (*vide infra:* dipolar attenuation).

Ensemble averaging is also a prerequisite to explain the modulation depth (observation *III*). In DEER4, the modulation depth λ accounts for the fraction of spin pairs with inverted partner spin. With probability λ, the modulated contribution of an individual spin pair therefore adds a contribution of the form of Eq. (2) to the ensemble-averaged DEER4 signal. With probability $(1-\lambda)$, the contribution to the signal has the form of Eq. (4). In the nDEER4 experiment, individual spin pairs contribute according to Eqs. (3) and (5) with probability λ and $(1-\lambda)$, respectively. This can be expressed mathematically as

$$V_{\mathrm{DEER4}}(t)|_{\mathrm{pairs}} = \lambda \cdot \langle \cos(\omega_{12} \cdot t) \rangle + (1-\lambda) \cdot \langle 1 \rangle \quad (6)$$

$$V_{\mathrm{nDEER4}}(t)|_{\mathrm{pairs}} = \lambda \cdot \langle \cos(\omega_{12} \cdot (t - \tau_2 + \tau_1)) \rangle + (1-\lambda) \cdot \langle \cos(\omega_{12} \cdot \tau_{\mathrm{sum}}) \rangle \quad (7)$$

where the brackets indicate ensemble averaging over ω_{12}. Eq. (6) corresponds to the DEER4 signal obtained with ideal pulses from an ensemble of spin pairs without any geometrical correlations (orientation selection) and without intermolecular couplings (background decay). The shape of this idealized DEER4 signal is well known and it is often referred to as the DEER form factor, which is the signal obtained after background-correction of primary experimental data[6]. As long as ideally selective pulses can be assumed[40], the modulation depth λ can be extracted with high accuracy from experimental DEER4 data. In essence, background-correction and data normalization in DEER4 results in the form factor which reaches an amplitude of 1.0 at $t = 0$, as prescribed by Eq. (6). This aspect is different in nDEER4, where the form factor according to Eq. (7) never reaches an amplitude of 1.0 for $\lambda < 1$. The reason for this is the non-modulated contribution with weight $(1-\lambda)$, which is attenuated by dipolar dephasing over the time period τ_{sum}. This renders extraction of λ from experimental nDEER4 data difficult. In particular, background-correction and normalization of nDEER4 data results in an *apparent* nDEER4 form factor with maximum amplitude of 1.0, which has a larger peak amplitude than the actual nDEER4 form factor in Eq. (7). As a consequence, the apparent nDEER4 modulation depth is larger than the *real* modulation depth λ in Eq. (7), which is related to the fraction of inverted spin partners.

While the extraction of λ from the apparent nDEER4 form factor is not trivial, it is important to notice that the modulated contributions of DEER4 and nDEER4 have the same weighting factor λ. The two techniques thus intrinsically provide identical modulation amplitudes λ. Accordingly, the larger apparent modulation depth in nDEER4 as compared to DEER4 (observation *III*) is due to attenuation of the non-modulated contribution, and it is not related to differences in the actual modulation amplitude.

The fact that our experiment showed an even larger dipolar modulation amplitude when going from DEER4 to nDEER4 (see Fig. 2d) is explained by the excitation bandwidth of the pulses that are used in the experiment. In particular, the broader bandwidth with chirp refocusing results in a larger fraction of spins contributing to the nDEER4 modulation than to the DEER4 modulation. When comparing datasets that reflect the amplitude of the raw echo signal, as in Fig. 2d, this emerges as a further enhancement of the modulation amplitude. While this is an important experimental aspect, it is not the reason why the apparent nDEER4 modulation depth is so much larger than the DEER4 modulation depth.

An additional experimental aspect to be mentioned is the pair-labeling efficiency, which accounts for molecules where only one of the two spins is attached. With the partner spin missing, the Hamiltonian in Eq. (1) does no longer apply. In general, this means that singly-labeled molecules will contribute differently to the signal. For the case here, singly-labeled molecules contribute by an unmodulated contribution of amplitude 1.0 for both experiments, which formally corresponds to Eq. (4). This implies that in DEER4, the contribution of a singly-labeled molecule is equal to the contribution of a doubly-labeled molecule where the parter spin is not inverted by the pump pulse. As a consequence of this, the labeling efficiency f attenuates λ and gives rise to an effective modulation depth $\lambda' = f\lambda$ of the DEER4 form factor[42]. If this effective λ' is substituted into Eq. (6), non-ideal labeling can readily be accounted for based on the modulation formula derived for a pair of spins.

Such a substitution of λ' is not possible in nDEER4. In particular, the unmodulated contribution in nDEER4 is attenuated due to dephasing by $\omega_{12}\tau_{\mathrm{sum}}$, which is no longer the case for a singly-labeled molecule. One would therefore expect that nDEER4 experiments performed with molecules that are difficult to label result in a rather pronounced unmodulated contribution. Dipolar modulation is then superimposed by a large unmodulated background, as for instance seen in Fig. S4 in the ESI†. While this significantly changes the appearance of the primary experimental data, it is important to notice that also for non-ideal labeling, the relevant modulated contribution of nDEER4 and DEER4 is of the same strength.

3.2.2 Modulation formula for three spins. Observation *IV* is related to the inter-molecular background decay in nDEER4. The incorporation of inter-molecular couplings requires a more complicated spin topology than the spin pair considered in the previous section. To keep the analysis as comprehensible as possible, we thus add one single spin to the scope of our problem and only focus on the relevant dipolar pathways that serve to explain the nDEER4 background decay. A more general modulation formula for multiple spins and related discussions are given in Section 3 of the ESI†. Adopting the notation from the previous section, the Hamiltonian thus becomes

$$\begin{aligned}\hat{\mathscr{H}}_0 &= \Omega_1\hat{S}_{1,z} + \Omega_2\hat{S}_{2,z} + \Omega_3\hat{S}_{3,z} \\ &\quad + \omega_{12}\hat{S}_{1,z}\hat{S}_{2,z} + \omega_{13}\hat{S}_{1,z}\hat{S}_{3,z} + \omega_{23}\hat{S}_{2,z}\hat{S}_{3,z}\end{aligned} \tag{8}$$

where ω_{13} is the dipolar coupling between spins 1 and 3, and ω_{23} is the dipolar coupling between spins 2 and 3. In general, there are a number of dipolar evolution pathways for such a three-spin system[43]. Without loss of generality, we here only consider the case where spin 1 acts as observer spin, whereas spins 2 and 3 are non-observed spins that are eventually flipped by the pump pulse. The observed spin is therefore subject to dipolar evolution under the coupling ω_{12} to its intra-molecular partner spin, as well as to evolution under the coupling ω_{13} to a remote spin residing on another molecule. For such a configuration, there are four different contributions to the ensemble-averaged signal:

i. Neither S_2 nor S_3 are inverted by the pump pulse

ii. Only S_2 is inverted by the pump pulse

iii. Only S_3 is inverted by the pump pulse

iv. Both S_2 and S_3 are inverted by the pump pulse

To write down the ensemble-averaged modulation formula, we assume that each of the spins S_2 or S_3 is inverted by the pump pulse with probability λ. Hence, we obtain an expression that formally corresponds to a previously derived three-spin modulation formula[43]

$$\begin{aligned}V_{\mathrm{DEER4}}(t)|_{3\mathrm{spin}} &= (1-\lambda)^2 \cdot \langle 1 \qquad\qquad \cdot 1\rangle \\ &\quad + \lambda(1-\lambda)\cdot\langle \cos(\omega_{12}\cdot t)\cdot 1\rangle \\ &\quad + (1-\lambda)\lambda\cdot\langle 1 \qquad\qquad \cdot\cos(\omega_{13}\cdot t)\rangle \\ &\quad + \lambda^2 \cdot \qquad \langle\cos(\omega_{12}\cdot t)\cdot\cos(\omega_{13}\cdot t)\rangle\end{aligned} \tag{9}$$

where the four lines in the equation correspond to the four cases *i*-*iv* stated above. Here, the brackets indicate ensemble averaging over ω_{12} and ω_{13}. The two factors in each bracket denote the pair-wise contributions related to these two dipolar frequencies, respectively. These pair-wise contributions are either unmodulated at an amplitude of 1.0, or modulated at the corresponding dipolar oscillation frequency.

Notice that if ω_{12} and ω_{13} are not correlated, the pair-wise contributions related to the intra-molecular and the inter-molecular spin partner can be averaged separately. In this case, Eq. (9) corresponds to the product of pair-wise contributions according to Eq. (6). This is the principle behind the well-known factorization of DEER data into an inter-molecular and an intra-molecular contribution[5]. For macromolecules shock-frozen into glassy matrices, it is indeed very reasonable to assume no correlation between the inter- and intra-molecular conformations.

For nDEER4, the modulation formula has the same structure, but different pair-wise contributions in the brackets. In particular,

$$\begin{aligned}V_{\mathrm{nDEER4}}(t)|_{3\mathrm{spin}} &= (1-\lambda)^2\cdot\langle\cos(\omega_{12}\cdot\tau_{\mathrm{sum}})\cdot\cos(\omega_{13}\cdot\tau_{\mathrm{sum}})\rangle \\ &\quad + \lambda(1-\lambda)\cdot\langle\cos(\omega_{12}\cdot t') \quad\cdot\cos(\omega_{13}\cdot\tau_{\mathrm{sum}})\rangle \\ &\quad + (1-\lambda)\lambda\cdot\langle\cos(\omega_{12}\cdot\tau_{\mathrm{sum}})\cdot\cos(\omega_{13}\cdot t')\rangle \\ &\quad + \lambda^2\cdot \qquad \langle\cos(\omega_{12}\cdot t') \quad\cdot\cos(\omega_{13}\cdot t')\rangle\end{aligned} \tag{10}$$

where we made use of the variable substitution $t' = t - \tau_2 + \tau_1$. Comparing the pair-wise contributions inside the brackets of Eqs. (9) and (10), one observes the following two features when substituting selective refocusing pulses by non-selective pulses. The first feature is that the refocusing times of the modulated pathways are shifted from $t = 0$ to $t = \tau_2 - \tau_1$. This aspect was used to explain observation *I* for a spin pair in Section 3.2.1. The second feature is that the unmodulated nDEER4 pathways do no longer have amplitude 1.0, but acquired phase over the entire pulse sequence duration, which introduces *dipolar attenuation*. In Section 3.2.1, dipolar attenuation for spin pairs explained observations *II* and *III*. As we will discuss in the following, it is this dipolar attenuation that explains the background behavior observed experimentally.

For the three-spin system considered here, the time-dependent background decay corresponds to contributions that are modulated by ω_{13}. There are two such contributions in the modulation formulas, namely lines *iii* and *iv*. Each of these two cases has distinct experimental consequences:

For case *iii*, the background decay is paired with the unmodulated constant contribution of the intra-molecular partner. Contributions of this type thus result in the apparent background decay observed in primary experimental data, i.e. the apparent curvature in primary experimental data. For case *iv*, the background decay is paired with the ω_{12} modulation. Such a pairing results in combination frequencies between ω_{13} and ω_{12}, which introduces broadening of the dipolar spectrum. In general, contributions of this type result in a more pronounced decay of the time-domain modulation in primary experimental data, as compared to the pure inter-spin modulation by ω_{12}. Since the experimenter has no *a priori* knowledge on the exact

shape of the ω_{12} modulation, contributions of the type *iv* are difficult to identify in primary experimental data.

When comparing cases *iii* and *iv* between DEER4 and nDEER4, one recognizes that contributions according to *iii* are attenuated when changing from DEER4 to nDEER4. Nevertheless, contributions of the type *iv* that introduce broadening of dipolar spectra have identical amplitudes in nDEER4 and DEER4. Our analysis therefore suggests that it is only the apparent background curvature that is suppressed when going from DEER4 to nDEER4, which explains observation *IV*. Contrary to the suppressed background curvature, however, dipolar broadening caused by the background decay is not altered considerably when going from DEER4 to nDEER4.

While we here only considered a three-spin system with one single inter-molecular spin partner, this concept can be extrapolated to multiple remote spins. In general, the apparent background curvature is connected to evolution pathways where the intra-molecular spin partner is not flipped by the pump pulse. In nDEER4, dipolar attenuation suppresses any of these contributions. Since these suppressed pathways have a probability weighting $(1-\lambda)$, the overall impact to the appearance of experimental data is significant. The implications of this partial background suppression are discussed in Section 3 of the ESI†, where generalized modulation formulas are derived, and below in Section 3.3.

While cases *iii* and *iv* in the three-spin modulation formulas above explain the background behavior, it is also important to consider cases *i* and *ii*. In particular, these contributions introduce dipolar attenuation due to remote inter-molecular spin partners. Since these remote partners are at a larger distance, this type of attenuation is expected to be rather weak for the molecule concentrations used within this study. In Section 4 in the ESI†, this expectation is confirmed by comparing DEER4 and nDEER4 data recorded from a mono-disperse solution of nitroxide radicals. In addition to these supplementary results, it is also noted that the experimental results in Fig. 2d virtually exclude a significant loss due to dipolar attenuation by inter-molecular spin partners. In particular, the principal ω_{12} modulation was visibly larger for nDEER4 as compared to DEER4, since the chirp refocusing pulses result in a larger echo bandwidth. In presence of a strong suppression effect introduced by inter-molecular spin partners, the nDEER4 modulation would be smaller than the DEER4 modulation.

3.2.3 Interference due to chirp refocusing. An aspect so far not considered is the influence of the frequency-swept chirp refocusing pulses in nDEER4 on spin dynamics. In particular, these pulses invert different spin packets at different times. This does not correspond to a hypothetical hard pulse that inverts all spin packets simultaneously. In fact, all the modulation formulas derived in the previous sections are only strictly valid for such an idealized hard pulse. In the following, we discuss under which conditions the modulation formulas derived so far also apply for the frequency-swept refocusing pulses used in our experiment. On the one hand, the frequency-progressive chirp excitation has an influence on the evolution of the resonance offset, which affects echo formation. On the other hand, the chirp pulse inverts the coupled spin partners one after another, which modifies the dipolar evolution pathways.

With respect to the resonance offset, it is well known that a pair of identical refocusing pulses compensates the chirp effects. In particular, this was first recognized in the context of NMR imaging experiments[44] and later on generalized to a pair of arbitrary refocusing pulses[45]. Importantly, the pair-wise compensation does not only refocus the frequency-progression of the chirp excitation, but it also removes transient Bloch-Siegert phase shifts induced by the refocusing pulses. The suppression of such Bloch-Siegert shifts has two advantages. First, it diminishes signal losses due to spatial inhomogeneity in the driving field ν_1. Second, it diminishes phase errors in echo spectra due to the offset-dependence of the Bloch-Siegert shift. Recently, we have observed that these Bloch-Siegert phase shifts have a linear dependence on the adiabaticity Q_{crit} of the refocusing pulse[23], which suggests that there is a general mechanism behind the transient phase shifts exerted by frequency-swept refocusing pulses.

For the dipolar evolution pathways, compensation of chirp effects by a pair of refocusing pulses is possible under certain conditions (see below). In order to consider this compensation effect with two refocusing pulses, the potential interference brought by one single refocusing pulse is analyzed first. It is noted that dipolar evolution throughout a frequency-swept non-selective refocusing pulse has already been considered in the analysis of the SIFTER experiment[28]. The basic effect is that, unlike a hard non-selective pulse, which inverts both spin partners simultaneously, the chirp pulse results in a non-zero delay δ_{12} in-between the inversion of the two spin partners. While the dipolar evolution throughout the pulse is unaffected for a hard non-selective pulse, the delay δ_{12} will refocus dipolar evolution during a total time period of $2\delta_{12}$. The bottom insets in Fig. S1 in the ESI† illustrate this effect. Accordingly, each refocusing pulse in nDEER4 will shorten the dipolar evolution phase by $\omega_{12}\delta_{12}$, as compared to the phase that would be acquired for a hard pulse.

In general, the potential complication introduced by δ_{12} is that the spectral distribution of the observed and pumped spins results in a distribution of δ_{12} times. If the spread in δ_{12} affects the resultant dipolar modulation and becomes comparable to the dipolar evolution period $2\pi/\omega_{12}$, the different contributions to the dipolar modulation interfere and complicate data analysis. For the particular case of nDEER4, however, the delay δ_{12} does not affect the modulated contribution. In fact, the inversion of the coupling Hamiltonian by the pump pulse in-

between the two refocusing pulses balances the chirp-induced phase loss $\omega_{12}\delta_{12}$ of each refocusing pulse: While the first pulse causes a phase loss of $\pm\omega_{12}\delta_{12}$, the second pulse causes a loss of $\mp\omega_{12}\delta_{12}$ (See also Fig. S1 in the ESI†). Independent on the value of δ_{12}, evolution under the coupling thus refocuses at $t' = 0$.

With respect to the nDEER modulation formulas derived so far, all factors that contribute to the nDEER modulation are thus also valid for chirp refocusing pulses. Nevertheless, such mutual compensation of δ_{12} is no longer possible in the absence of the pump pulse. In this case, the phase losses of each pulse add up to a total loss of $2\omega_{12}\delta_{12}$ (or $2\omega_{12}\delta_{13}$). To account for this in the derived modulation formulas, one would therefore need to subtract this phase factor in each cosine function that constitutes dipolar attenuation and therefore depends on τ_{sum}. In the ESI† in Section 2, the distribution of δ_{12} for our experimental conditions is estimated. As shown in Fig. S2 in the ESI†, the distribution is centered around δ_{12} = 10 ns and has an overall spread of 20 ns. This timescale is negligibly small as compared to τ_{sum}, so that it can be neglected and the formulas derived so far are also applicable for chirp refocusing.

In summary, the delay δ_{12} introduced by each of the non-selective refocusing pulses can only be compensated pair-wise if the coupling Hamiltonian is inverted in-between, as it is the case for nDEER4. In the CP nDEER pulse sequences presented below in Section 4, pair-wise compensation will no longer hold throughout the entire pulse sequence.

Notice also that under certain circumstances, it is possible to combine frequency-swept pulses with opposite sweep directions to compensate chirp effects in the evolution under spin-spin couplings[46], as exemplified for DEER with multiple pump pulses[18]. However, these strategies rely on excitation schemes where the chirp pulse excites solely the pumped spins, which excludes the non-selective chirp refocusing encountered here. In particular, the delay δ_{12} has no dependence on the sweep direction of the refocusing pulse.

3.3 Discussion

Based on our experimental results and theoretical analysis, we conclude that the substitution of the selective refocusing pulses in DEER4 by non-selective pulses has three main consequences. The first consequence is the shift of the zero time of the dipolar oscillation. While this largely influences the primary appearance of experimental data, this time shift does not manifest in a significant distinction between DEER4 and nDEER4.

The second consequence is that the non-selective chirp refocusing pulses in nDEER4 refocus the observer spins more efficiently than the selective counterparts in DEER4. This results in a larger amplitude and bandwidth of the resulting nDEER4 modulation as compared to DEER4, which is advantageous in terms of the signal-to-noise ratio (SNR) and in terms of potential complications due to imperfections of the refocusing pulses.

The third consequence is the dipolar attenuation introduced by unobserved spin partners that are not inverted by the pump pulse. It is this property which makes a clear distinction between the spin dynamics of DEER4 and of nDEER4. In particular, some dipolar evolution pathways are attenuated more than others, which introduces a filtering effect in nDEER4 that is not present in DEER4.

The net filtering depends strongly on the topology of the spin system under investigation and also on the inversion efficiency λ of the pump pulse. For nitroxides at Q-band frequencies, one operates close to $\lambda = 0.5$. In this regime, it is quite probable to *not* flip a coupled partner spin, since $1-\lambda \approx \lambda \approx 0.5$. With the coupled partner spin not flipped, the corresponding evolution pathways are suppressed by the aforementioned dipolar attenuation.

The spin topology of our model compound corresponds to dilute spin pairs, which is a topology encountered in many studies involving pair-wise spin-labeling of biomacromolecules. In this case, dipolar attenuation by the spatially close partner spin on the same molecule introduces significant suppression of any dipolar evolution pathway that is not contributing to the principal dipolar oscillation. These suppressed contributions include the apparent curvature in primary experimental data due to the inter-molecular background, as well as all non-modulated contributions. This filtering has both advantages and disadvantages:

The advantage of the filtering is that the primary experimental nDEER4 signal comes close to the principal dipolar oscillation that is of interest for pair-wise distance determination. Potential complications due to the correction of the apparent curvature during post-processing are thus expected to be smaller for nDEER4 as compared to DEER4. In particular, incomplete correction of the background curvature results in artificial contributions at long distances. While the suppressed background curvature reduces the uncertainty with respect to such artificial contributions, it enhances the uncertainty with respect to broadening of the dipolar spectrum. In particular, the intra-molecular dipolar spectra in nDEER4 and DEER4 experience comparable broadening by the inter-molecular dipolar spectrum. In DEER4, this broadening is removed by dividing primary data by the inter-molecular background decay extracted from primary data[5]. In nDEER4, the background decay as extracted from primary data is less pronounced, so that division by the suppressed background decay does not completely remove the aforementioned broadening (see also Section 3 in the ESI†). In order to keep this residual broadening negligible, nDEER4 is therefore dedicated to systems where the intra-molecular contribution decays much faster than the inter-

molecular contribution. In this work, the compounds were diluted to 50 μM. As we will show further below in Section 4, no significant broadening could be detected when comparing nDEER4 to DEER4 at these concentrations. However, one would expect that larger concentrations or local crowding result in significant broadening.

Shortcomings related to the filtering in nDEER4 are that information related to the suppressed contributions is more difficult to extract. In particular, the unmodulated contribution of amplitude 1.0 in DEER4 allows for an estimate of the modulation depth, which is no longer the case in nDEER4. In particular, quantification of the modulation depth allows to estimate the pair-wise labeling efficiency[42] or the number of intra-molecular spin partners[47], given that the pump pulses are well characterized. Moreover, suppression of the background curvature in nDEER4 makes it difficult to extract the *true* background decay from nDEER4 data. Besides the above mentioned aspect related to deconvolution of background broadening from dipolar spectra, knowledge of the background decay provides insight into the intra-molecular topology. In particular, extraction of the background decay in DEER4 provides insight into the local molecule concentration[48–50]. For the molecule concentration around 50 μM used in this work, the residual background decay in nDEER data was removed using automatic background correction in DeerAnalysis 2016[51] (see below in Fig. 4b). For this correction, a stretched exponential function is fitted to the nDEER decay in such a way as to minimize artificial contributions at long distances. Further data is required to verify if this strategy also works at larger concentrations and for different spin geometries.

Other than the spin topology of diluted spin pairs, it is worth to consider the filtering for another common topology, namely molecules with more than two spin labels. In this case, there is more than one intra-molecular spin parter that is effective in suppressing dipolar pathways that do not contribute to its modulation. The least attenuated pathway is therefore the one where all intra-molecular spin partners are inverted by the pump pulse. This corresponds to the highest possible mixing product in a multi-spin system[42,43]. On multi-spin systems, nDEER4 therefore favors the largest combination products. This is opposite to DEER4, where one usually tries to avoid the presence of any combination products[42]. nDEER4 has therefore the potential to provide complementary information on such multi-spin systems.

4 Dynamical decoupling by multiple refocusing

In this section, experimental schemes that combine non-selective DEER with dynamical decoupling are presented. The principal aspects of the nDEER modulation, as discussed in the previous Section, remain unchanged when incorporating dynamical decoupling. We thus aim for sequences that provide the same information content as nDEER4, but with enhanced sensitivity due to dynamical decoupling.

The main motivation to incorporate dynamical decoupling schemes into DEER is to prolong the phase memory time to access longer distances[29]. Existing approaches rely on selective refocusing pulses which refocus the observer spins. Since the timing of these refocusing pulses has an influence on the dipolar evolution throughout the sequence, the incorporation of CP pulse trains into DEER requires multiple pump pulses for best use of the available time window. In particular, a CP train with N refocusing pulses in DEER requires the same number of pump pulses[29]. The total number of pulses for CP DEER is therefore $2N+1$.

Due to the introduction of multiple pump pulses, these CP DEER schemes entail a specific challenge. In particular, the intended CP DEER evolution pathway requires the pumped spins to be flipped by each of the N pump pulses. The pump pulse should therefore be highly frequency selective, meaning that the pulse should invert spins inside its excitation window with an efficiency of 100%, while not affecting spins outside its excitation window. Even when using pump pulses with hyperbolic-secant modulation functions, which in theory are highly frequency selective, the intended evolution pathway is superimposed by unwanted pathways[30]. These artifact pathways complicate data analysis in CP DEER. Another aspect related to $N > 2$ pump pulses is that the generation of the time axis by the pump pulses to acquire t is not necessarily straightforward to understand.

With non-selective refocusing, the timing of the refocusing pulses does not influence the dipolar evolution throughout the refocusing pulse. This provides more flexibility in the implementation of CP nDEER and ultimately allows to use a smaller number of pulses for a given number N of refocusing pulses as in CP DEER (see below).

The results below in Section 4.1 are presented as follows. First, Section 4.1.1 presents the actual implementation of a CP refocusing train with $N = 2$ and $N = 4$ pulses into nDEER. In this context, peculiar features that are specific to the CP nDEER implementation and apparent in primary experimental data are taken into consideration. Section 4.1.2 then addresses the quality of CP nDEER data. In particular, this section assesses the relative intensity of unwanted artifact pathways achievable with non-selective refocusing. This assessment is initiated with a comparison of experimental data obtained with CP nDEER, nDEER4 and DEER4. Then, Section 4.1.3 shows to which extent a larger number of non-selective refocusing pulses in CP nDEER is advantageous.

4.1 Results

4.1.1 CP2-nDEER and CP4-nDEER pulse sequences. The observer sequence with $N = 2$ non-selective refocusing

pulses is shown in the top of Fig. 3a. Besides the pulses, the primary and the refocused primary echo are indicated by the Gaussian profiles. The primary echo is broader in time domain, because it corresponds to a frequency-progressive spin echo, whereas the refocused primary echo is narrower since all spin packets refocus at the same time[44,52]. The delay between the two refocusing pulses is parametrized by the variable τ. Since the refocusing pulses are non-selective, the pump spin is also inverted. The $\pi/2-\pi-\pi$ subsequence has therefore no influence on the evolution of the dipolar coupling, except for the small correction due to chirp refocusing pulses discussed in Section 3.2.3. The observed spins thus dephase under the dipolar interaction throughout the entire sequence duration 2τ. In presence of the selective pump pulse placed at a delay τ with respect to the first pulse, the dipolar interaction is refocused and the net dipolar phase is controlled by changing the position of the pump pulse along the black arrow. As this arrow indicates, the pump pulse is shifted ahead of the first refocusing pulse. The pump pulse is therefore moving *through the refocusing pulse*, while avoiding direct pulse overlap. If this pulse skip would not be implemented, the CP2-nDEER sequence would correspond to nDEER4 with timing $\tau_1=\tau_2=\tau/2$. Such a sequence could only acquire the dipolar evolution up to $t=\tau/2$, which is half of the maximum available time window. By skipping the refocusing pulse, the CP2-nDEER pulse sequence makes use of virtually the entire time window available and remains dead-time free. In fact, the time t in CP2-nDEER can be incremented up to the point where the pump pulse immediately follows the first pulse.

Notice that in CP DEER with two selective refocusing pulses, an analogous situation has been encountered: DEER4 with CP timing of $\tau_1=\tau_2=\tau/2$ could only acquire the dipolar evolution up to $t=\tau/2$, which has been solved by introduction of a second pump pulse in the five-pulse DEER experiment[29]. A conceptual difference remains between the introduction of an additional pump pulse in CP DEER and pulse skipping in CP nDEER. In particular, the pump pulse in CP2-nDEER can, in principle, be placed at any timing $-\tau<t<\tau$. The CP2-nDEER modulation can thus always acquired be up to the maximum $t=\tau$, independent on the how many data points for negative times $t<0$ are acquired. Hypothetically, one could acquire a symmetric CP2-nDEER modulation, as it is for instance possible in DQC and SIFTER experiments. In five-pulse DEER, the maximum possible evolution time $t=\tau$ is offset by the small number of data points recorded at $t<0$. Nevertheless, moving the pump pulse through the first refocusing pulse in CP nDEER constrains the choice of the time increment Δt, such that direct overlap of pulses is avoided. As described in Section 2.2, our short and intense refocusing pulses allowed for $\Delta t=96$ ns. In addition, the pair-wise refocusing of the delay δ_{12} is no longer compensated if the pump pulse is no longer placed in-between the two refocusing pulses

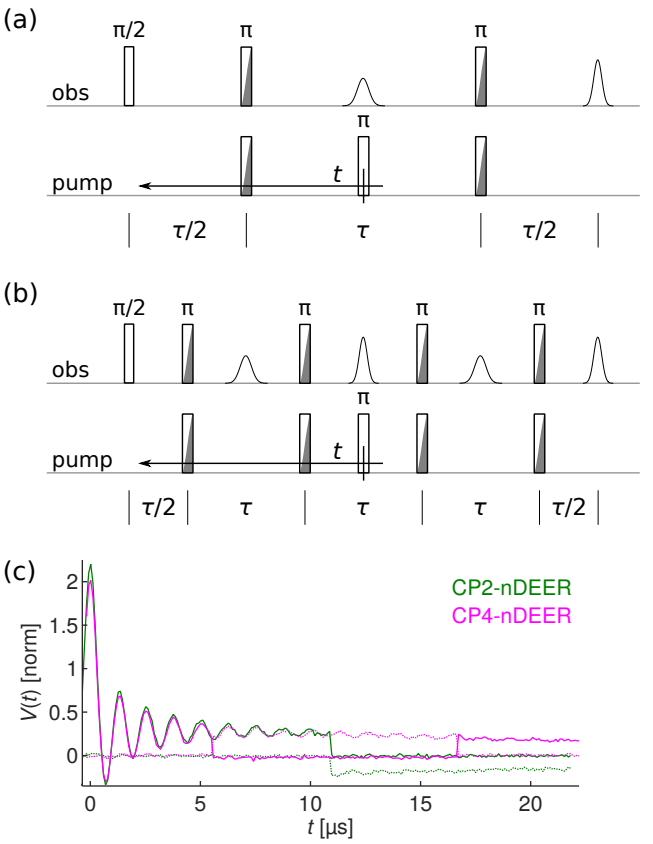

Fig. 3 nDEER sequences with dynamical decoupling. **(a)** CP2-nDEER sequence with two non-selective chirp refocusing pulses. The pump-only pulse position is stepped from right to left, while avoiding direct overlap with all other pulses. The evolution time t of the principal modulation has its zero in the middle of the sequence, as marked by the vertical line. **(b)** CP4-nDEER sequence with four non-selective chirp refocusing pulses, where $t=0$ is also in the middle. **(c)** Raw signals $V(t)$ for CP2-nDEER (green) and CP4-nDEER (magenta), showing both the real (solid) and imaginary (dotted) components. Both curves are normalized to the echo intensity obtained with a nDEER4 experiment at the same evolution time (see below in Fig. 4). The delays τ between the refocusing pulses were set to 21.888 μs and 11.136 μs for CP2-nDEER and CP4-nDEER, respectively, and 27 scans were averaged each.

(see Section 3.2.3). The nDEER modulation is thus affected by a net uncertainty in the time axis of $2\delta_{12}$ for $|t|>\tau/2$. For our experimental parameters, this corresponds to an uncertainty of 40 ns (see Section 2 in ESI†).

The extension of CP2-nDEER to CP4-nDEER is straightforward and is illustrated in Fig. 3b. Dipolar evolution is analogous as in CP2-nDEER, which means that the pump pulse is now moving through both the second and the first refocusing pulse. With four refocusing pulses, the total uncertainty in the time t is increased from 40 ns to 80 ns. In particular, af-

ter skipping one single refocusing pulse at $|t| > \tau/2$, the time axis adopts the same uncertainty of $2\delta_{12}$ as in CP2-nDEER. After skipping also the second refocusing pulse at $|t| > 3\tau/2$, the uncompensated contribution from all refocusing pulses enhances the uncertainty to $4\delta_{12}$.

Primary experimental data for CP2-nDEER (green) and CP4-nDEER (purple) are shown in Fig. 3c, where details on the pulse sequence timing τ are given in the caption. The depicted real (solid) and imaginary (dotted) components were normalized to the maximum echo amplitude obtained in a nDEER4 experiment with identical dipolar evolution time (see below). As is readily seen, there are abrupt phase jumps in the primary data. These are related to the transient Bloch-Siegert phase shift induced by the pump pulse on the observed spins[53]. In particular, this shift is either positive or negative, depending on the number of refocusing pulses in-between the first excitation pulse and the pump pulse. Skipping over the refocusing pulses thus changes the sign of the transient phase shift. Since the echo phase of experimental data was determined at $t = 0$, the phase jumps of CP2-nDEER and CP4-nDEER are in opposite directions. This is explained by the different number of refocusing pulses, which precede the pump pulse at $t = 0$.

As detailed in the ESI† in Section 5, these phase jumps can be removed rather well using a root-mean-square minimization of the imaginary component related to each of the two segments. While this procedure resulted in continuous data for CP4-nDEER, the amplitude of the CP2-nDEER signal turned out to be attenuated after skipping the refocusing pulse. This amplitude jump was observed in all CP2-nDEER data, is currently not understood, and was corrected for during post-processing. Further discussions on this aspect are found in the ESI† in Section 5, where all phase and amplitude jumps are also analyzed by considering the spectral impurity of the sample tube that was co-recorded during each experiment.

4.1.2 Data quality achieved by CP nDEER. In order to assess the quality of CP nDEER data, CP2-nDEER and CP4-nDEER data are compared to DEER4 and nDEER4. Consequently, the CP2-nDEER and CP4-nDEER data corrected according to the procedures detailed in the ESI† are shown in Fig. 4a, using the same colors as in Fig. 3. Raw data obtained for DEER4 (orange) and nDEER4 (blue) at identical evolution times t are also shown, where the time axis of nDEER4 was adjusted according to its zero time. The enhancement of the echo amplitude due to the CP pulse train becomes evident when comparing echo amplitudes of CP2-nDEER and CP4-nDEER with nDEER4.

Processing of these experimental datasets with DeerAnalysis 2016[51] resulted in the data shown in panels (b) - (d). In particular, panel (b) shows the background corrected form factors, which were scaled and vertically displaced to provide unity modulation amplitude. These curves allowed to compare the SNR of the various experiments and revealed an SNR improvement of at least two when going from DEER4 to either CP2-nDEER or CP4-nDEER. Panels (c) and (d) illustrate the dipolar spectrum and regularized distance distributions. Within experimental uncertainty, all four experiments revealed the same distance information. Nevertheless, there are some tiny differences seen on a close look at the main peak in the

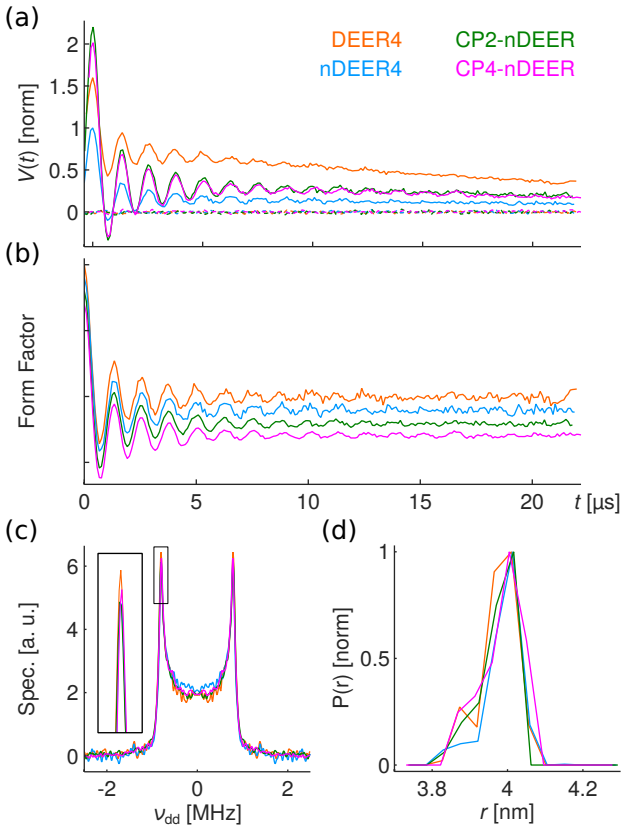

Fig. 4 Comparison of DEER4 (orange), nDEER4 (blue), CP2-nDEER (green), and CP4-nDEER (magenta). DEER4 and nDEER4 had $\tau_1 = 400$ ns and $\tau_2 = 22$ μs. The time axis t of nDEER4 was adjusted according to the zero time of the dipolar modulation. The timing of CP2-nDEER and CP4-nDEER was as described in Fig. 3. All data acquired with 27 scans each. **(a)** Real (solid) and imaginary (dashed) components of $V(t)$, where raw CP2-nDEER and CP4-nDEER data from Fig. 3c were corrected as described in the text. All signals are normalized to the nDEER4 echo amplitude. **(b)** Form factors obtained by automatic background fitting within DeerAnalysis 2016[51]. All form factors are normalized to unity modulation and displaced vertically. **(c)** Dipolar spectra of the form factors in panel b, where the inset shows a zoom of the peak. **(d)** Regularized distance distributions normalized to maximum intensity each. Selection of regularization parameters using the L-curve criterion[54,55] resulted in small parameters, namely [0.26, 0.26, 0.15, 0.11], respectively.

dipolar spectrum (see zoom inset). In particular, this peak was largest for DEER4, which could in principle be an effect related to broadening of the nDEER spectra by the residual background decay (see Section 3). However, the DEER4 trace also features a rather pronounced modulation refocusing at the end of the trace due to the second refocusing pulse acting as a non-selective pulse[40], which also contributes to the main dipolar peak. In any case, these small differences in the spectra did not result in a significant change of the resulting distance distributions, even at the extraordinary small regularization parameters used here.

However, the introduction of multiple non-selective refocusing pulses is prone to artifacts. In particular, the non-selective refocusing pulses have an inversion efficiency below 100% (see Fig. 2b). There is therefore a finite probability that the refocusing pulses do not invert either the pumped or the observed spins. If the observed spins are not refocused, there is no contribution to the relevant echo due to the phase cycle used here (see Section 2.2). If the pumped spins are not inverted by the refocusing pulse, the dipolar evolution pathway is altered. In fact, nDEER with a N-pulse CP train relies on $N+1$ flips of the pumped spins. Here, the N flips are realized by the broadband refocusing pulses that invert the spins almost adiabatically. The additional '+1' flip is done by the pump pulse. The chance for the chirp pulse to not flip a pumped spin is on the order of 2% - 4%, as deduced from the experimental pulse characterization in Fig. 2b. In the ESI† in Section 6, we analyze the dipolar evolution of all relevant artifacts both experimentally and theoretically. Moreover, we characterize the artifact level in our experiments by comparing CP2-nDEER and CP4-nDEER data in Section 7 of the ESI†. The artifact level observed in these data confirms that the probability for not flipping a pumped spin was indeed below 4%.

Having identified the positions where the unwanted dipolar evolution pathways refocus, it is actually possible to recognize these artifacts in the data presented in Fig. 4b. In particular, the CP4-nDEER modulation had the most extended dipolar oscillations among the performed experiments, which is well perceived on a close look at the oscillations during the last quarter of the evolution window. In fact, the modulation peak around 16.5 μs had a larger amplitude than its two adjacent modulation peaks. With respect to the resulting distance distribution, these artificial modulations may also explain the smaller regularization parameter (see caption). This extended artificial oscillation for CP4-nDEER is also the reason why the spectral peak of CP4-nDEER was slightly stronger than the overlapping peaks of CP2-nDEER and nDEER4 (see zoom inset).

4.1.3 Efficiency of dynamical decoupling. The results shown in Fig. 4 revealed the largest echo amplitude for the CP2-nDEER experiment, while CP4-nDEER had a slightly

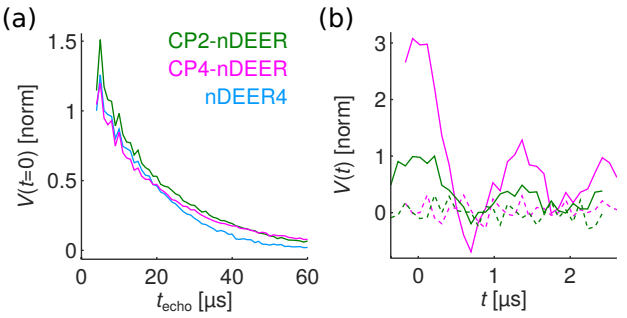

Fig. 5 Prolongation of coherence time in nDEER by dynamical decoupling. **(a)** Dependence of nDEER echo $V(t=0)$ with refocused dipolar evolution on sequence length t_{echo} for nDEER4 (blue), CP2-nDEER (green), and CP4-nDEER (magenta). The pulse delays τ for CP2-nDEER and CP4-nDEER were set to a half and a quarter of t_{echo}, respectively. For nDEER4, $\tau_2 = t_{\mathrm{echo}}/2 - \tau_1$ with τ_1 = 400 ns. Each dataset was acquired during 14 min and reached up to t_{echo} = 100 μs. Results shown in Figs. 3 and 4 were acquired at t_{echo} around 44 μs. **(b)** Initial modulation acquired with CP2-nDEER (green) and CP4-nDEER (magenta) with τ set to 43.776 μs and 22.080 μs, respectively. With respect to panel b, these data correspond to t_{echo} around 88 μs. Data acquired for 20 min each (10 scans).

smaller amplitude. In the following, we examine the origin of the observed amplitudes. In particular, Fig. 5a shows the decay of the relevant echo as a function of the overall pulse sequence time t_{echo} for the three nDEER experiments, where the same colors as in Figs. 3 and 4 were used. The timings for this experiment are detailed in the caption. Importantly, the depicted curves correspond to the echo where the dipolar evolution was refocused, such that echo decays were acquired with the pump pulse at the corresponding zero position.

By comparing CP2-nDEER with nDEER4, the advantage of the CP pulse spacing with respect to the fluctuating nuclear spin environment encountered in our model sample is observed. In particular, the CP2-nDEER echo was strictly larger than the nDEER4 echo. When going from an $N = 2$ to an $N = 4$ CP pulse train, one would expect that dynamical decoupling is further improved[31,32]. This manifests in a less steep echo decay as a function of t_{echo}. When comparing CP4-nDEER to CP2-nDEER, this is indirectly seen in the data. In particular, the CP4-nDEER decay starts at short t_{echo} with a smaller echo intensity since the refocusing pulses are non-ideal. Despite the smaller intensity at the start, the CP4-nDEER echo becomes larger than the CP2-nDEER echo for $t_{\mathrm{echo}} > 47$ μs. The improved dynamical decoupling when going from $N = 2$ to $N = 4$ is thus indeed observed. Notice that the experiments presented in Sections 4.1.1 and 4.1.2 were performed around $t_{\mathrm{echo}} = 44$ μs, which explains why CP2-nDEER had a larger echo amplitude than CP4-nDEER in these

experiments.

Notice further that the ortho-terphenyl matrix is per-deuterated and causes an extraordinarily long phase memory time of 21 μs already in the absence of dynamical decoupling.

An important observation is that while the change from $N = 2$ to $N = 4$ refocusing pulses results in a less steep decay, the efficiency of the refocusing pulses may offset the potential gain when increasing N. In this respect, the chirp refocusing pulses employed here are advantageous as compared to the monochromatic refocusing pulses used in previous CP DEER experiments[29,30,33]. This becomes apparent when comparing the pulse excitation profiles in Fig. 2b, where much larger inversion efficiency was obtained for the chirp refocusing pulse. In Section 8 of the ESI†, we compare the echo decay with non-selective refocusing shown in Fig. 5a to the corresponding echo decay with selective monochromatic refocusing, where the latter resulted in a more pronounced performance reduction.

In order to demonstrate that there is a potential for significant signal enhancement when changing from CP2-nDEER to CP4-nDEER for $t_{\mathrm{echo}} > 47$ μs, we recorded the initial part of the CP2-nDEER and CP4-nDEER modulation for t_{echo} around 88 μs (see Fig. 5b). This corresponds to pulse sequences with twice the pulse spacings τ as in the previous sections. Due to a gating limitation of our high-power amplifier, we only activated the amplifier when a pulse was sent to the amplifier and disabled it in-between pulses (see also Section 2.2 and Section 5 of ESI†).

When comparing the CP4-nDEER modulation in Fig 5b to the CP2-nDEER modulation, the sensitivity improvement is on the order of 3. Even at this long pulse sequence duration, the improvement related to the echo intensity at $t = 0$ translates into a corresponding improvement in the modulation amplitude. Notice that this is not necessarily the case for the sample studied here due to the E' centers in the sample tube, which have a longer phase memory time than the nitroxide labels and could introduce offsets. In order to avoid such complications, high-temperature annealing of the clear fused quartz tube prior to sample insertion is recommended.

4.2 Discussion

Overall, CP pulse trains by non-selective chirp refocusing have proven to be very promising for distance determination. In particular, the CP nDEER pulse sequences require a smaller number of pulses than CP DEER for a given number N of refocusing pulses ($N+2$ vs. $2N+1$). Only the first excitation pulse and the pump pulse are selective and determine the observed and the pumped spin packets. The refocusing pulses do not need to be frequency-selective, so that short and intense pulses allow for inversion performance close to the adiabatic limit. DEER schemes with multiple pump pulses on the contrary rely on multiple selective pulses, whose non-ideal excitation profiles result in accumulation of significant artifacts throughout the pulse sequence.

The superior rejection of artifacts related to pulse imperfections in nDEER allowed to perform experiments with $N = 4$ refocusing pulses and analyze the data without corrections for artificial dipolar modulations. In fact, these residual dipolar modulations contributed only by 3.5%. We are currently not aware of CP DEER experiments with $N = 4$ refocusing pulses. In addition, the experiments presented with $N = 2$ and $N = 3$ refocusing pulses contained larger artificial modulations, which required dedicated data processing or experimental schemes to recover the modulation of interest[18,29,30].

The time incrementing scheme of the pump pulse in CP nDEER is easier to understand than for CP DEER and also makes use of the maximum possible time window. However, the unique pulse skipping employed in nDEER also has its disadvantages. In particular, primary data was affected by large phase jumps and in some cases also by detectable amplitude jumps after skipping a pulse (see ESI†). The phase jumps are related to Bloch-Siegert phase shifts and could be removed reliably using an automated phase correction. Amplitude jumps are not that well understood and were most significant for CP2-nDEER with $N = 2$ refocusing pulses, while virtually absent for CP4-nDEER with $N = 4$ refocusing pulses. For CP2-nDEER, the jump was adjusted below the noise level by an amplitude correction. Notice that both the phase and the amplitude jumps observed experimentally affected a series of data points by a complex multiplication factor. Such a constant multiplication factor is easier to correct than a time-dependent artificial modulation caused by pulse imperfections. In particular, amplitude offsets beyond the noise level are readily recognized by the residual to a fit to experimental data computed with established DEER data analysis software.

Pulse skipping also constrains the minimum time increment Δt of the pump pulse. One could circumvent this limitation by also changing the position of the refocusing pulse during the pulse skip. In this way, the pulse skip is realized by the time increment Δt by the pump pulse accomplished by a larger step Δ_{nonsel} into the other direction. The pitfall of such an approach is that the shifting of the refocusing pulse position by Δ_{nonsel} is prone to introduce an amplitude jump. Another way to circumvent the limitation on the minimum Δt is to utilize two pump pulses instead of one. In this way, the lost time gap while skipping a refocusing pulse can be compensated by moving the second pump pulse. Indeed, both these approaches require versatile pulse sequence programming. In a preliminary implementation of nDEER, we performed pulse skipping by two pump pulses (data not shown). Besides introducing spurious dipolar modulation pathways, a serious limitation of this approach was related to the Bloch-Siegert phase jumps

that are also observed with a single pump pulse. In particular, pulse skipping with multiple pump pulses resulted in constellations where the Bloch-Siegert shifts exerted by each of the pump pulses were either added together or compensated by subtraction. This resulted in very pronounced amplitude jumps, since the compensation of Bloch-Siegert phase shifts alleviates losses introduced by spatial inhomogeneity of the driving field[23,45].

As it seems difficult to remove the limitation on the minimum time increment Δt without introducing additional complications, the minimum Δt of 96 ns imposes a restriction on distances shorter than 3 nm, whose modulation pattern would require a shorter time increment. We would expect that for most systems, where dynamical decoupling is beneficial in terms of sensitivity, the distance range is beyond this limitation from Δt. Note also that we consider the limitation due to Δt to be more severe with respect to short distances than the uncertainty in the time axis due to interference from chirp excitation. While pulse skipping progressively enhances this uncertainty, it is absent up to the first pulse skip. With respect to the dampened modulation patterns that are encountered in spin-labeled molecules, the most critical initial decay around $t = 0$ is thus not affected by interference from chirp excitation.

For the fluctuating nuclear spin environment encountered in our model compound, CP nDEER techniques prolonged the potential sequence duration into a regime where limitations due to the power amplifier were encountered. Clearly, the attainable sequence duration strongly depends on the actual nuclear spin environment and little is currently known about this aspect. For proton-containing environments, faster decays are expected, where instrumental limitations are no longer an issue. In general, the optimum number N of refocusing pulses can be chosen by selecting the sequence that achieves the largest echo for the required sequence duration. For systems that exhibit faster relaxation decays than encountered in this study, the optimum number N may be larger than 4. With the efficient suppression of residual dipolar modulations achieved by nDEER, we would not expect significant additional complications when going to CP6-nDEER or even higher. In many practical applications, the spurious dipolar modulation by 3.5% would be on the order of the noise level. One critical limitation when increasing the number of refocusing pulses may be encountered for systems that exhibit pronounced nuclear modulation effects due to forbidden transitions, which are also excited by chirp refocusing pulses[23,56,57]. In particular, the CP timing of the refocusing pulses could enhance such modulation effects[58].

With respect to potential broadening by incomplete deconvolution of the inter-molecular background decay, we note that the CP nDEER techniques face the same limitations as discussed for nDEER4 in Section 3.3. The concentration should thus be kept at a small level. For the primary purpose of CP nDEER, which is the determination of long distances, it is worth to notice that dilute spin concentrations as encountered in this study are also favorable in ordinary DEER experiments[5]. In particular, the sensitivity problem that arises when determining long distances is not solved by increasing concentration and dilute samples with a weak background decay are favored.

5 Summary

The substitution of non-selective refocusing pulses into DEER pulse sequences selects a dipolar evolution pathway with unique characteristics. In particular, non-selective refocusing leads to suppression of unmodulated contributions to the nDEER signal, which is an effect that we refer to as dipolar attenuation. The attenuation strength depends on the topology of the spin cluster under investigation.

The most common topology corresponds to pairs of spins diluted in a disordered solid. In this case, primary nDEER and DEER data encode the same principal dipolar oscillation. Nevertheless, primary DEER and nDEER data emerge differently, because the non-modulated contributions are attenuated in nDEER. On the one hand, the loss of these non-modulated contributions in nDEER is connected to a loss of complementary information that is available in DEER. On the other hand, the principal dipolar oscillation that is relevant for distance determination can be recorded at a larger sensitivity using nDEER. Especially the extension to dynamical decoupling with a CP train of refocusing pulses renders nDEER a promising technique for extending the range of accessible distances. To the best of our knowledge, the presented CP nDEER experiments so far feature the best rejection of unwanted evolution pathways related to pulse imperfections. Accordingly, CP nDEER at the performance of our Q-band spectrometer does not require additional post-processing to correct for these unwanted pathways, at least up to the $N = 4$ refocusing pulses realized in this study.

As highlighted in the theoretical analysis of nDEER, a potential complication of nDEER data analysis is related to the deconvolution of broadening effects due to the inter-molecular background. Notably, this broadening effect is present in both DEER and nDEER data. However, dipolar attenuation hinders the extraction from primary nDEER data. At present, the scope of nDEER is therefore limited to systems that are diluted to local concentrations as encountered in this study (50 μM) or lower, where broadening effects were not resolved. Further research towards these broadening effects may also stimulate alternate approaches for background deconvolution for both DEER and nDEER.

Other than the topology of diluted spin pairs, biomacromolecules may feature a network of more than two coupled spin partners. In this case, it is important to note that theory

predicts the principal oscillations of DEER and nDEER to be different. In particular, dipolar attenuation introduces a filtering effect that prefers the pathway where all coupled spin partners contribute to the modulation. Accordingly, nDEER on systems with multiple inter-molecular spin partners provides complementary information to DEER for use in structure determination.

6 Acknowledgements

We are thankful to René Tschaggelar and Oliver Oberhänsli for the design and construction of the loop-gap resonator. Muhammad Sajid and Adelheid Godt are acknowledged for the synthesis of the rigid model compound. Fruitful discussions on DEER with multiple selective monochromatic refocusing with Frauke Breitgoff and Janne Soetbeer are acknowledged. This work was supported by the Swiss National Science Foundation (SNSF grant No. 20020_157034). Andrin Doll acknowledges a mobility grant by the SNSF for research abroad.

References

1 G. Jeschke and Y. Polyhach, *Phys. Chem. Chem. Phys.*, 2007, **9**, 1895–1910.
2 O. Schiemann and T. F. Prisner, *Q. Rev. Biophys.*, 2007, **40**, 1–53.
3 G. Jeschke, *Annu. Rev. Phys. Chem.*, 2012, **63**, 419–446.
4 P. P. Borbat and J. H. Freed, in *Structure and Bonding*, ed. C. R. Timmel and J. R. Harmer, Springer Berlin Heidelberg, 2013, vol. 152, pp. 1–82.
5 G. Jeschke, *eMagRes*, 2016, **5**, 1–18.
6 M. Pannier, S. Veit, A. Godt, G. Jeschke and H. Spiess, *J. Magn. Reson.*, 2000, **142**, 331 – 340.
7 A. Milov, K. Salikhov and M. Shirov, *Sov. Phys. Solid State*, 1981, **23**, 565–569.
8 A. Schweiger and G. Jeschke, *Principles of Pulse Electron Paramagnetic Resonance*, Oxford University Press, USA, 2001.
9 V. Yudanov, K. Salikhov, G. Zhidormirov and Y. Tsvetkov, *Theor. Exp. Chem.*, 1972, **5**, 451–455.
10 P. P. Borbat and J. H. Freed, *Chem. Phys. Lett.*, 1999, **313**, 145 – 154.
11 G. Jeschke, M. Pannier, A. Godt and H. Spiess, *Chem. Phys. Lett.*, 2000, **331**, 243 – 252.
12 P. P. Borbat and J. H. Freed, in *Distance Measurements in Biological Systems by EPR*, ed. L. J. Berliner, G. R. Eaton and S. S. Eaton, 2002, vol. 19, pp. 383–459.
13 G. B. Park and R. W. Field, *J. Chem. Phys.*, 2016, **144**, 200901.
14 J. S. Hodges, *Ph.D. thesis*, Massachusetts Institute of Technology, 2007.
15 M. Tseitlin, R. W. Quine, G. A. Rinard, S. S. Eaton and G. R. Eaton, *J. Magn. Reson.*, 2011, **213**, 119 – 125.
16 P. E. Spindler, Y. Zhang, B. Endeward, N. Gershernzon, T. E. Skinner, S. J. Glaser and T. F. Prisner, *J. Magn. Reson.*, 2012, **218**, 49 – 58.
17 A. Doll, S. Pribitzer, R. Tschaggelar and G. Jeschke, *J. Magn. Reson.*, 2013, **230**, 27 – 39.
18 P. E. Spindler, S. J. Glaser, T. E. Skinner and T. F. Prisner, *Angew. Chem. Int. Ed.*, 2013, **52**, 3425–3429.
19 M. Garwood and L. DelaBarre, *J. Magn. Reson.*, 2001, **153**, 155 – 177.
20 J. Baum, R. Tycko and A. Pines, *Phys. Rev. A*, 1985, **32**, 3435–3447.
21 F. D. Giacomo and E. E. Nikitin, *Phys. Uspekhi*, 2005, 515.
22 J. W. Zwanziger, S. P. Rucker and G. C. Chingas, *Phys. Rev. A*, 1991, **43**, 3232–3240.
23 G. Jeschke, S. Pribitzer and A. Doll, *J. Phys. Chem. B*, 2015, **119**, 13570–13582.
24 A. Doll, M. Qi, S. Pribitzer, N. Wili, M. Yulikov, A. Godt and G. Jeschke, *Phys. Chem. Chem. Phys.*, 2015, **17**, 7334–7344.
25 A. Doll, M. Qi, N. Wili, S. Pribitzer, A. Godt and G. Jeschke, *J. Magn. Reson.*, 2015, **259**, 153 – 162.
26 *J. Magn. Reson.*, 2016, **273**, 73 – 82.
27 P. Schöps, P. E. Spindler, A. Marko and T. F. Prisner, *J. Magn. Reson.*, 2015, **250**, 55 – 62.
28 A. Doll and G. Jeschke, *Phys. Chem. Chem. Phys.*, 2016, **18**, 23111–23120.
29 P. P. Borbat, E. R. Georgieva and J. H. Freed, *J. Phys. Chem. Lett.*, 2013, **4**, 170–175.
30 P. E. Spindler, I. Waclawska, B. Endeward, J. Plackmeyer, C. Ziegler and T. F. Prisner, *J. Phys. Chem. Lett.*, 2015, **6**, 4331–4335.
31 H. Y. Carr and E. M. Purcell, *Phys. Rev.*, 1954, **94**, 630.
32 J. Du, X. Rong, N. Zhao, Y. Wang, J. Yang and R. Liu, *Nature*, 2009, **461**, 1265–1268.
33 C. E. Tait and S. Stoll, *Phys. Chem. Chem. Phys.*, 2016, **18**, 18470–18485.
34 M. Sajid, G. Jeschke, M. Wiebcke and A. Godt, *Chem. Eur. J.*, 2009, **15**, 12960–12962.
35 G. Jeschke, M. Sajid, M. Schulte, N. Ramezanian, A. Volkov, H. Zimmermann and A. Godt, *J. Am. Chem. Soc.*, 2010, **132**, 10107–10117.
36 A. Doll and G. Jeschke, *J. Magn. Reson.*, 2014, **246**, 18 – 26.
37 J. M. Böhlen and G. Bodenhausen, *J. Magn. Reson.*, 1993, **102**, 293 – 301.
38 O. Sørensen, G. Eich, M. H. Levitt, G. Bodenhausen and R. Ernst, *Prog. Nucl. Magn. Reson. Spectrosc.*, 1984, **16**, 163–192.
39 R. Freeman, S. P. Kempsell and M. H. Levitt, *J. Magn. Reson.*, 1979, **35**, 447 – 450.
40 K. Salikhov and I. Khairuzhdinov, *Appl. Magn. Reson.*, 2015, **46**, 67–83.
41 V. V. Kurshev, A. M. Raitsimring and Y. D. Tsvetkov, *J. Magn. Reson.*, 1989, **81**, 441 – 454.
42 T. von Hagens, Y. Polyhach, M. Sajid, A. Godt and G. Jeschke, *Phys. Chem. Chem. Phys.*, 2013, **15**, 5854–5866.
43 G. Jeschke, M. Sajid, M. Schulte and A. Godt, *Phys. Chem. Chem. Phys.*, 2009, **11**, 6580–6591.
44 S. Conolly, G. Glover, D. Nishimura and A. Macovski, *Magn. Reson. Med.*, 1991, **18**, 28–38.
45 K. E. Cano, M. A. Smith and A. Shaka, *J. Magn. Reson.*, 2002, **155**, 131 – 139.
46 E. Kupĉe and R. Freeman, *J. Magn. Reson.*, 1997, **127**, 36 – 48.
47 B. E. Bode, D. Margraf, J. Plackmeyer, G. Dürner, T. F. Prisner and O. Schiemann, *J. Am. Chem. Soc.*, 2007, **129**, 6736–6745.
48 A. Milov, K. Salikhov and M. Shirov, *Fiz. Tverd. Tela*, 1981, **23**, 975–982.
49 A. Milov, A. Maryasov and Y. D. Tsvetkov, *Appl. Magn. Reson.*, 1998, **15**, 107–143.
50 D. R. Kattnig, J. Reichenwallner and D. Hinderberger, *J. Phys. Chem. B*, 2013, **117**, 16542–16557.
51 G. Jeschke, V. Chechik, P. Ionita, A. Godt, H. Zimmermann, J. Banham, C. Timmel, D. Hilger and H. Jung, *Appl. Magn. Reson.*, 2006, **30**, 473–498.
52 R. Bhattacharyya and L. Frydman, *J. Chem. Phys.*, 2007, **127**, 194503.
53 M. K. Bowman and A. G. Maryasov, *J. Magn. Reson.*, 2007, **185**, 270 – 282.
54 G. Jeschke, G. Panek, A. Godt, A. Bender and H. Paulsen, *Appl. Magn. Reson.*, 2004, **26**, 223–244.
55 Y.-W. Chiang, P. P. Borbat and J. H. Freed, *J. Magn. Reson.*, 2005, **172**, 279 – 295.
56 T. F. Segawa, A. Doll, S. Pribitzer and G. Jeschke, *J. Chem. Phys.*, 2015,

143, 044201.
57 S. Pribitzer, T. F. Segawa, A. Doll and G. Jeschke, *J. of Magn. Reson.*, 2016, **272**, 37 – 45.
58 G. Mitrikas and G. Prokopiou, *J. Magn. Reson.*, 2015, **254**, 75 – 85.